# Isotropic second-order dipolar shifts in the rotating frame

Matthias Ernst, Andrew C. Kolbert,[a] Klaus Schmidt-Rohr,[b] and Alexander Pines
*Materials Sciences Division, E. O. Lawrence Berkeley National Laboratory, Berkeley, California 94720 and Department of Chemistry, University of California, Berkeley, California 94720*

(Received 21 December 1995; accepted 26 February 1996)

An experiment is described that utilizes the truncation of the Hamiltonian in the rotating frame by a radio-frequency field designed to yield an isotropic shift for the dipolar coupling. This approach allows the measurement of a normally orientation-dependent coupling constant by a single isotropic value. The dipolar isotropic shift is closely related to the field-dependent chemical shift in solids due to the second-order dipolar perturbation observed in magic-angle spinning experiments. In the rotating frame, larger shifts of up to 1000 Hz can be observed for the case of a one-bond C–H coupling compared to a shift of a few Hertz in the laboratory-frame experiment. In addition to the isotropic shift, a line broadening due to the $P_4(\cos\beta)$ terms is observed when the experiment is carried out under magic-angle sample spinning (MAS) conditions, leading to the requirement of higher-order averaging such as double rotation (DOR) for obtaining narrow lines. As an application of this new experiment the separation of CH, $CH_2$, and $CH_3$ groups in a 2D spectrum under MAS is demonstrated. Implemented under DOR it could be used as a technique to select carbon atoms according to the number of directly attached protons. © *1996 American Institute of Physics.* [S0021-9606(96)00221-8]

## I. INTRODUCTION

Truncation of laboratory-frame Hamiltonians by a static Zeeman field[1,2,3] is a very important concept in high-field nuclear magnetic resonance (NMR) spectroscopy. The Hamiltonian is transformed into a frame rotating with the Zeeman frequency of the nuclei, the zero-order or static terms are retained and all higher-order terms are neglected. This approximation works well if the Zeeman interaction is much larger than all terms in the internal Hamiltonian and is often referred to as the high-field approximation.[2,3] It is certainly recognized that this approximation is not always adequate to describe a spin system and in such cases higher-order terms must be included in the rotating-frame Hamiltonian. The next level of approximation is to include all terms derived from second-order static perturbation theory, the so-called second-order corrections.[2,3] In the average Hamiltonian approach[2–5] these terms show up in the first-order average Hamiltonian. In the laboratory frame the second-order contributions to the Hamiltonian are proportional to $\omega_i^2/\omega_z$, where $\omega_i$ is the strength of the interaction and $\omega_z$ is the Zeeman frequency. This leads in many cases to a field-dependent chemical shift inversely proportional to the $B_0$-field which can be used to identify second-order effects. Higher-order terms can be calculated but are rarely used since they are much smaller and not important at high fields.

One example of an important second-order effect in the laboratory frame is the quadrupolar interaction in high magnetic fields.[6] Since quadrupolar-coupling constants can be as large as several megahertz,[6] the second-order terms cannot always be neglected even for the highest Zeeman fields currently available. This effect is known as the second-order quadrupolar shift[6] and leads to a $B_0$-field dependent isotropic shift in spectra of quadrupolar nuclei and an additional anisotropy which transforms as the sum of a second- and a fourth-rank tensor. To eliminate the resulting broadening requires the use of dynamic-angle spinning (DAS) or double rotation (DOR) techniques[7,8,9] or the combined use of multiple-quantum spectroscopy and magic-angle sample spinning.[10]

A second important example of a second-order effect in the laboratory frame is the Bloch–Siegert shift.[2,3,11] A strong rf-field off-resonance from a nuclear Larmor frequency causes an rf-field-dependent shift.[2,3,12] The shifts are usually small except in the case of spin decoupling for two nuclei with very similar Larmor frequencies, as in the case of $^{19}F-^{1}H$ double-resonance experiments. In such cases, shifts of several ppm have been observed.[13]

Some years ago, a Zeeman field-dependent isotropic shift in solids was observed under magic-angle sample spinning (MAS) and proton decoupling;[14] the effect was interpreted as a dipolar shift arising from the second-order contribution of the heteronuclear dipolar couplings. The observed shifts are in the order of a few Hertz for a one-bond C–H coupling at a typical $B_0$-field of 4.7 T and can therefore be neglected for most practical purposes. The effect has been analyzed in terms of the Floquet formalism[15] and it has been shown that the shift is accompanied by a broadening of the same order of magnitude as the shift.

The same effect should be observable for the symmetric part of the chemical-shielding tensor if the $B_0$-field is not along one of the principal axes of the chemical-shielding tensor and for the antisymmetric part as well. Both induce fields orthogonal to the $B_0$-field[16,17] and can therefore give rise to a second-order effect, which would show up as a field-dependent chemical shift. To our knowledge, no experi-

[a]Present address: DSM Copolymer Inc., P.O. Box 2591, Baton Rouge, Louisiana 70821.
[b]Present address: Department of Polymer Science and Engineering, University of Massachusetts, Amherst, Massachusetts 01003.

 0021-9606/96/104(21)/8258/11/$10.00 

mental proof of this effect has been reported in the literature.

We have performed and analyzed an experiment closely related to the field-dependent dipolar shift, which exploits the second-order effects in the rotating frame. Using the rf-field to truncate the interaction is often referred to as second averaging[2] and has the advantage that the observed second-order effects are not scaled by the Zeeman interaction, $\omega_z^{-1}$, but by the rf-field, $\omega_{\rm rf}^{-1}=(\gamma B_1)^{-1}$. The $B_1$-fields are typically three to four orders of magnitude smaller than the $B_0$-field and lead therefore to much larger second-order effects than the laboratory-frame experiments. For the case of a one-bond C–H dipolar coupling we have calculated and observed second-order shifts of up to 1000 Hz for a field strength of $\omega_{\rm rf}/(2\pi)=100$ kHz compared to a shift of a few Hertz observed commonly in the laboratory-frame experiment.[14,15] The experiment is related to the zero-field NMR experiment at high fields.[18] However, there the goal is to generate an isotropic dipolar-coupling Hamiltonian at high fields, whereas in our experiment the anisotropic dipolar coupling is transformed into an isotropic shift in the rotating frame.

A common feature of all second-order effects is that they depend on the square of the interaction tensor scaled by the size of the truncating field. If the interaction itself transforms as a second-rank tensor, the square of the interaction can be decomposed into a sum of a scalar, a second-rank tensor, and a fourth-rank tensor.[19] The scalar part is the part which gives rise to the isotropic shift. The second- and fourth-rank tensors are responsible for the observed powder broadening which is always associated with the second-order shift. The powder broadening of the lines can be eliminated partially by MAS or completely by DOR.

The material is presented as follows. In Sec. II we analyze the most straightforward implementation of the proposed experiment and present numerical simulations (static, MAS, and DOR) to show the basic features of the second-order dipolar shift in the rotating frame. An improved version of the experiment is then analyzed within the framework of average Hamiltonian theory. In Sec. III we show an experimental realization of this technique and demonstrate a potential application to separate the signals of CH, $CH_2$, and $CH_3$ groups in a 2D spectrum under MAS.

## II. THEORETICAL CALCULATIONS AND NUMERICAL SIMULATIONS

### A. Basic theory

The basic experiment that we are considering is a simple nutation experiment (Fig. 1) where we observe the nutation frequency of the spin during $t_1$ under an applied rf-field of strength $\omega_{\rm rf}=\gamma B_1$. Assuming a static heteronuclear two-spin system ($S-I$) and neglecting the chemical-shielding tensor, we can describe the Hamiltonian in the rotating frame during $t_1$ by

$$\mathscr{H}=\omega_D(\Omega)\cdot 2S_zI_z+\omega_{\rm rf}\cdot S_x. \tag{1}$$

The orientation-dependent second-rank dipolar-coupling tensor is

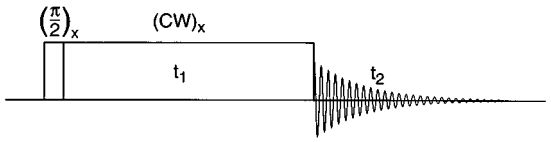


FIG. 1. Basic pulse sequence which can be used to measure the second-order dipolar isotropic shift in the rotating frame. After an initial $(\pi/2)_x$-pulse the magnetization precesses about a rf-field along $+x$ during $t_1$ and is then detected during $t_2$. The experiment can be transformed into a phase-sensitive version by the addition of another $(\pi/2)_x$-pulse after $t_1$ to generate the second data set needed for States-type processing.

$$\omega_D(\Omega)=-\frac{\mu_0}{4\pi}\cdot\frac{\gamma_S\gamma_I\hbar}{r_{SI}^3}\cdot P_2(\cos\beta)$$
$$=\frac{\delta}{2}\cdot P_2(\cos\beta), \tag{2}$$

$P_2(\cos\beta)$ is the second-rank Legendre polynomial, and $\Omega=(\alpha,\beta,\gamma)$ is a set of three Euler angles describing the orientation of the dipolar-coupling tensor in the laboratory frame. We can analytically diagonalize this Hamiltonian and for an initial state of

$$\sigma(0)=S_y \tag{3}$$

and under a phase-sensitive detection operator

$$D=S_y+i\cdot S_z \tag{4}$$

we obtain two transition frequencies during $t_1$,

$$\omega_\pm(\Omega)=\pm\omega_{\rm rf}\sqrt{1+\left[\frac{\omega_D(\Omega)}{\omega_{\rm rf}}\right]^2}. \tag{5}$$

The corresponding signal intensities are

$$S(\omega_\pm)=\frac{1}{4}\left\{1\pm\sqrt{1+\left[\frac{\omega_D(\Omega)}{\omega_{\rm rf}}\right]^2}\right\}. \tag{6}$$

These two lines represent the nutation frequency and the corresponding quadrature image, because the effective nutation axis is slightly tilted off the $x$-axis due to the influence of the dipolar coupling. If we assume that the field strength $\omega_{\rm rf}$ is substantially larger than the maximum value of the dipolar-coupling tensor $\omega_D(\Omega)$, we can expand the square root in Eq. (5) in a power series and obtain

$$\omega_\pm(\Omega)=\pm\omega_{\rm rf}\cdot\left\{1+\frac{1}{2}\left[\frac{\omega_D(\Omega)}{\omega_{\rm rf}}\right]^2-\frac{1}{8}\left[\frac{\omega_D(\Omega)}{\omega_{\rm rf}}\right]^4+\frac{3}{48}\left[\frac{\omega_D(\Omega)}{\omega_{\rm rf}}\right]^6-\cdots\right\}. \tag{7}$$

Limiting this expansion to the first two terms is equivalent to a second-order static perturbation treatment. We can rewrite the square of the second-order Legendre polynomial as a sum of a zeroth-order, second-order, and fourth-order Legendre polynomial[19] to obtain the following expression:

$$\omega_D^2(\Omega) = \frac{\delta^2}{4}\,[P_2(\cos\,\beta)]^2$$

$$= \delta^2 \cdot \left[\frac{1}{20} + \frac{1}{14}\,P_2(\cos\,\beta) + \frac{9}{70}\,P_4(\cos\,\beta)\right]. \quad (8)$$

Substituting Eq. (8) into Eq. (7) and neglecting all higher-order terms in Eq. (7) leads to the following approximate expression for the nutation frequency:

$$\omega_{\pm}(\Omega) \approx \pm\left\{\omega_{\rm rf} + \frac{\delta^2}{2\omega_{\rm rf}} \cdot \left[\frac{1}{20} + \frac{1}{14}\,P_2(\cos\,\beta) + \frac{9}{70}\,P_4(\cos\,\beta)\right]\right\}. \quad (9)$$

In addition to the expected nutation frequency $\omega_{\rm rf}$ we obtain another isotropic term $\delta^2/(40\omega_{\rm rf})$ which shows the inverse proportionality to the rf-field strength typical for second-order corrections. For a one-bond C–H coupling constant of $\delta/(2\pi)=46.6$ kHz and a rf-field strength of $\omega_{\rm rf}/(2\pi)=50$ kHz, we calculate a shift of 1086 Hz. Besides this isotropic contribution there are two orientation-dependent terms which transform as second- and fourth-rank tensors. They are the source of a broadening of the nutation spectra. Under static conditions we therefore expect a broad line due to the $P_2(\cos\beta)$ and $P_4(\cos\beta)$ terms in Eq. (9). These powder broadenings can be removed partially by recording the spectra under magic-angle spinning (MAS) (Refs. 20, 21, 22) or completely by double rotation (DOR). In this implementation of the experiment dynamic-angle spinning (DAS) could also be used to fully remove the second- and fourth-rank tensor powder broadenings.[7,8,9]

The above treatment is only correct if the rotation induced by the rf-field is substantially faster than the mechanical rotation due to MAS or DOR, i.e., if $\omega_{\rm rf} \gg \omega_r$. If the mechanical rotation is much faster than the rf-field, $\omega_{\rm rf} \ll \omega_r$, the order of the averaging processes has to be reversed and no second-order dipolar isotropic shift can be observed. In the intermediate regime where $\omega_{\rm rf} \approx \omega_r$, the system becomes complicated and a theoretical description is no longer possible in terms of consecutive averaging processes. In this case, a multimode Floquet[23] description or numerical simulations have to be used.

The Hamiltonian in Eq. (1) does not include the chemical-shielding tensor of both the $S$- and the $I$-spin. The chemical-shielding tensor of the $I$-spin has no influence on the observed transition frequencies or intensities. The $S$-spin chemical-shielding tensor, however, gives rise to basically the same type of shifts as the dipolar-coupling tensor, except for the presence of additional cross terms. The full Hamiltonian including both chemical-shielding tensors is

$$\mathscr{H} = \omega_D(\Omega) \cdot 2S_zI_z + \omega_S(\Omega_S) \cdot S_z + \omega_I(\Omega_I) \cdot I_z + \omega_{\rm rf} \cdot S_x, \quad (10)$$

where $\Omega_S$ and $\Omega_I$ are sets of Euler angles describing the relative orientation of the principal-axes systems (PAS) of the $S$- and $I$-spin chemical-shielding tensors, respectively, in the laboratory frame. The Hamiltonian of Eq. (10) leads to the following four transition frequencies:

$$\omega_m(\Omega, \Omega_S) = \pm\,\omega_{\rm rf}\sqrt{1 + \left[\frac{\omega_D(\Omega) \pm \omega_S(\Omega_S)}{\omega_{\rm rf}}\right]^2}. \quad (11)$$

Equation (11) can be expanded in a power series of the tensors and treated in a manner similar to the case of dipolar coupling shown in Eqs. (7)–(9).

### B. Numerical simulations

In order to analyze and verify the theoretical calculations in Sec. II A, we have performed numerical simulations on a heteronuclear two-spin system using the NMR-simulation package GAMMA.[24,25] Three different sets of simulations were performed under static, MAS, and DOR conditions. The coupling constant was set to $\delta/(2\pi)=46.6$ kHz, which corresponds to a one-bond C–H coupling of $r_{\rm CH}=1.09$ Å. No chemical-shielding tensor was included for either spin since the size of the shift induced by the chemical-shielding tensor is much smaller than the size of the shift induced by a one-bond C–H coupling. Assuming an anisotropy of the chemical-shielding tensor of $\delta=50$ ppm, a carbon resonance frequency of 100 MHz, and a rf-field strength of 90 kHz, we calculate an isotropic shift of 25 Hz compared to a shift of more than 1000 Hz induced by the dipolar coupling. The powder average was performed over 376 different orientations using the formalism of Cheng[26] to attain optimal coverage of the sphere. The static spectra were obtained by a frequency-domain simulation, which calculated the transition frequencies and probabilities. The spectra were convolved with a Gaussian line of width 100 Hz.

The MAS and DOR spectra were calculated using Floquet theory.[23,27,28] We can rewrite the time-independent Hamiltonian of Eq. (1) under magic-angle sample spinning in the following time-dependent form:

$$\mathscr{H}(t) = \omega_D(\Omega(t)) \cdot 2S_zI_z + \omega_{\rm rf} \cdot S_x$$

$$= \left[\sum_{m=-2}^{2} \mathscr{D}^2_{0,m}(\alpha,\beta,\gamma) \cdot d^2_{m,0}(\theta) \cdot e^{-im\omega_r t}\right] \cdot \frac{\delta}{2}$$

$$\cdot 2S_zI_z + \omega_{\rm rf} \cdot S_x = \sum_{m=-2}^{2} \mathscr{H}^{(m)} \cdot e^{-im\omega_r t}, \quad (12)$$

where $\mathscr{D}^2_{m,n}(\alpha,\beta,\gamma)$ are the Wigner rotation matrix elements[19] with the Euler angles $\alpha$, $\beta$, and $\gamma$ representing the orientation of the crystallite relative to the rotor-fixed frame; $d^2_{m,n}(\theta)$ is the reduced Wigner rotation matrix element;[19] $\theta$ is the angle of the sample rotation axis with the static magnetic field; $\omega_r$ is the spinning speed; and $\delta$ is the anisotropy of the dipolar coupling as defined in Eq. (2). The Floquet Hamiltonian is then given by[28]

$$\mathscr{H}^F = \sum_{\substack{n,m \\ \phi,\varphi}} |\phi,n\rangle\langle\phi|\mathscr{H}^{(n-m)}|\varphi\rangle\langle\varphi,m|, \quad (13)$$

where $|\phi,n\rangle$ are the composite basis function of the Floquet space. For the DOR spectra we perform a two-mode Floquet simulation[25,28] with

$$\mathscr{H}(t)=\sum_{m_1=-2}^{2}\sum_{m_2=-2}^{2}\mathscr{H}^{(m_1,m_2)}\cdot e^{-im_1\omega_1 t}\cdot e^{-im_2\omega_2 t}, \tag{14}$$

$$\mathscr{H}^{(m_1,m_2)}=\mathscr{D}^2_{0,m_1}(\alpha,\beta,\gamma)\cdot d^2_{m_1,m_2}(\theta_1)\cdot e^{-i\zeta m_2}\cdot d^2_{m_2,0}(\theta_2)\cdot\frac{\delta}{2}\cdot 2S_Z I_Z+\omega_{\mathrm{rf}}S_X\cdot\delta_{0,m_1}\cdot\delta_{0,m_2}, \tag{15}$$

and

$$\mathscr{H}^F=\sum_{\substack{n_1,n_2\\ m_1,m_2\\ \phi,\varphi}}|\phi,n_1,n_2\rangle\langle\phi|\mathscr{H}^{(n_1-m_1,n_2-m_2)}|\varphi\rangle\times\langle\varphi,m_1,m_2|. \tag{16}$$

$\mathscr{D}^2_{m,n}(\alpha,\beta,\gamma)$ are the Wigner rotation matrix elements[19] with the Euler angles $\alpha$, $\beta$, and $\gamma$ describing the orientation of the crystallite relative to the first rotor-fixed frame. $\theta_1$ and $\theta_2$ are the inclination angles of the two axes about which the sample is rotating with the frequencies $\omega_1$ and $\omega_2$, respectively. $\zeta$ is the phase difference between the two rotors, and $\delta_{m,n}$ is the Kronecker delta function. Numerical diagonalization of this Hamiltonian with the Floquet space limited to $|n-m|\leqslant 10$ (MAS) and $|n_1-m_1|\leqslant 4$, $|n_2-m_2|\leqslant 4$ (DOR) was used to calculate the frequency-domain spectrum under MAS or DOR using the appropriate density and detection operators[28] to obtain the relative intensities of the transition frequencies. Again a powder average over 376 (MAS) or 100 (DOR) different orientations was performed and the resulting spectra were convolved with a 100 Hz Gaussian line. The spinning speed was set to 5 kHz in the case of MAS and to 1 kHz and 5 kHz in the case of DOR.

Figure 2 shows the simulations for the static, MAS ($\theta=54.74°$), and DOR ($\theta_1=54.74°$, $\theta_2=30.12°$) case for four different field strengths $\omega_{\mathrm{rf}}/(2\pi)$ between 30 kHz and 90 kHz. The zero point of the frequency axis is always set to the basic nutation frequency $\omega_{\mathrm{rf}}/(2\pi)$ to facilitate a comparison of the spectra at different field strengths. In the static case, we see a broad line due to the superposition of the $P_2(\cos\beta)$ and $P_4(\cos\beta)$ powder patterns. The width of the line scales with the inverse of the field strength, $\omega_{\mathrm{rf}}^{-1}$. The MAS spectra show a much narrower line than the static spectra (note the different scale of the frequency axes in Fig. 2) with the expected $P_4(\cos\beta)$ powder pattern, which again scales with the inverse of the rf-field strength. The DOR spectra show a single sharp line with spinning sidebands. The isotropic position (i.e., the center of gravity) of all the spectra is shifted as can be seen best from the DOR spectra. This second-order shift scales linearly with the inverse of the field strength, $\omega_{\mathrm{rf}}^{-1}$, as expected from the theoretical calculations.

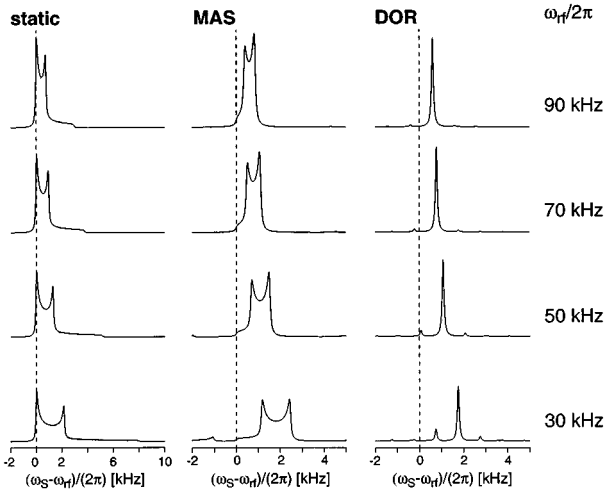


FIG. 2. Simulation of the second-order dipolar isotropic shift in the rotating frame for a dipolar-coupling constant of $\delta/(2\pi)=46.6$ kHz, corresponding to a C–H distance of $r_{\mathrm{CH}}=1.09$ Å. The powder averages were performed using 376 (static and MAS) or 100 (DOR) different orientations and the resulting frequency-domain spectra were convolved with a Gaussian line of width 100 Hz. In the MAS and DOR simulations, Floquet theory was used to describe the time-dependent Hamiltonian. The MAS rotation frequency was set to 5 kHz and the DOR frequencies were 1 kHz and 5 kHz. The origin of the frequency axis was set to the basic nutation frequency $\omega_{\mathrm{rf}}/(2\pi)$ in order to facilitate a comparison of the spectra at different field strengths. The DOR spectra exhibit clearly the dependence of the additional shift on the inverse rf-field strength. The broadening in the static and MAS spectra is due to the $P_2(\cos\beta)$ and $P_4(\cos\beta)$ powder orientation dependent terms which are averaged out by DOR. Note that the frequency axis for the static spectra is different from that for the MAS and DOR spectra. More details of these simulations can be found in the text.

### C. Improved experiment

The main shortcoming of the experiment as shown in Fig. 1 is its sensitivity to rf-field inhomogeneities. Since the desired effect is superimposed on the basic nutation frequency $\omega_{\mathrm{rf}}$, any inhomogeneity of the rf-field will lead to a substantial broadening of the resonance lines. For a solid-state NMR probe, we can expect a Gaussian distribution of the inhomogeneity with a width of roughly 5% of the rf-field strength.[29] In the case of a 100 kHz rf-field, the inhomogeneity would lead to a line with 5 kHz half-width which would make the observation of a shift of the order of 1 kHz very difficult.

In order to overcome this problem, we use a different type of nutation sequence which compensates for the nutation due to the rf-field but not that due to the second-order dipolar shift. Three different approaches to achieve this goal are shown in Fig. 3. They all rely on the fact that the rotation due to the second-order shift scales with the inverse of the field strength, $\omega_{\mathrm{rf}}^{-1}$, while the nutation due to the rf-field scales linearly with the field strength, $\omega_{\mathrm{rf}}$. Assuming that the inhomogeneity is proportional to the rf-field strength, these sequences will reduce the broadening due to rf-field inhomogeneities substantially. The sequence in Fig. 3(a) implements this by rotating the spins by $(2\pi)_x$ at a field strength $\omega_{\mathrm{rf}}$ and then back by $(2\pi)_{-x}$ at a lower field strength $a\times\omega_{\mathrm{rf}}$ where $a$

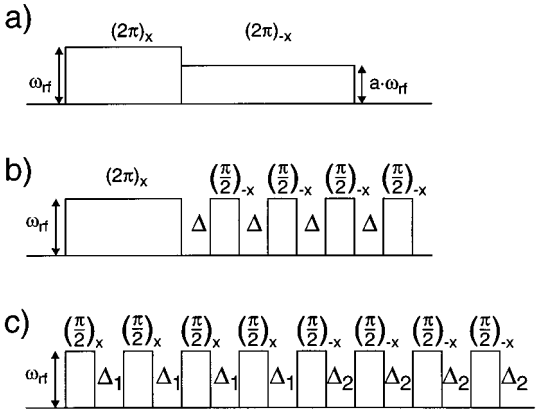


FIG. 3. Three different pulse schemes designed to implement the compensated version of the second-order dipolar shift experiment. In (a) a $(2\pi)_x$-pulse is followed by a $(2\pi)_{-x}$-pulse with lower rf-field strength. This leads to a compensation of the basic rotation due to the rf-field, but the rotation due to the second-order effect is retained because the second-order effect scales with $\omega_{\mathrm{rf}}^{-1}$ and not with $\omega_{\mathrm{rf}}$. In (b) the same effect is achieved by using four $(\pi/2)_{-x}$-pulses spaced by a delay $\Delta$. This leads to a lower effective field for the back rotation resulting again in a cancellation of the basic nutation frequency but not of the second-order effect. In (c) delays are inserted in both the forward and the back rotation. The delay $\Delta_1$ was usually set to 0.3 $\mu$s (the shortest possible value on our instrument) and $\Delta_2$ was varied to observe different dipolar shifts ensuring that the timing of the pulses for both rotations is the same and producing experimentally superior compensation of the basic nutation frequency than the sequence in (b).

is a scaling factor describing the relative intensities of the two applied rf-fields. The sequence in Fig. 3(b) achieves the same goal by inserting delays between the $(\pi/2)_{-x}$-pulses to create a lower time-averaged field for the back rotation. The practical implementation used in all the experiments presented in the next section is shown in Fig. 3(c). In this version delays are inserted between the $(\pi/2)_x$-pulses as well as between the $(\pi/2)_{-x}$-pulses. This has the advantage that the basic nutation due to the rf-field is better compensated than with the pulse sequence of Fig. 3(b).

We can analyze the Hamiltonian under the influence of these three pulse sequences most easily within the framework of average Hamiltonian theory (AHT).[2–5] In order to simplify the calculation of higher orders of average Hamiltonians, a program in *Mathematica*[30] using the spin-1/2 simulation package SOME (Ref. 31) was developed to analytically calculate the first four orders of average Hamiltonians for pulse sequences consisting of delays and pulses with arbitrary phases and amplitudes. Starting from the Hamiltonian in Eq. (10), we can calculate the zeroth to third order for the pulse sequence shown in Fig. 3(a),

$$\bar{\mathscr{H}}^{(0)} = \omega_I(\Omega_I)\cdot I_Z, \tag{17}$$

$$\bar{\mathscr{H}}^{(1)} = -\frac{1-a^2}{a^2+a}\cdot\left[\frac{\omega_D(\Omega)^2+\omega_S(\Omega_S)^2}{2\omega_{\mathrm{rf}}}\cdot S_X + \frac{2\omega_D(\Omega)\omega_S(\Omega_S)}{2\omega_{\mathrm{rf}}}\cdot 2S_XI_Z\right], \tag{18}$$

$$\bar{\mathscr{H}}^{(2)} = \frac{1+a^3}{a^3+a^2}\cdot\left[\frac{\omega_S(\Omega_S)^3+3\omega_S(\Omega_S)\omega_D(\Omega)^2}{2\omega_{\mathrm{rf}}^2}\cdot S_Z + \frac{\omega_D(\Omega)^3+3\omega_D(\Omega)\omega_S(\Omega_S)^2}{2\omega_{\mathrm{rf}}^2}\cdot 2S_ZI_Z\right], \tag{19}$$

$$\bar{\mathscr{H}}^{(3)} = \frac{1-a^4}{a^4+a^3}\cdot\left[\frac{3}{8}\cdot\frac{\omega_D(\Omega)^4+6\omega_D(\Omega)^2\omega_S(\Omega_S)^2+\omega_S(\Omega_S)^4}{\omega_{\mathrm{rf}}^3}\cdot S_X + \frac{3}{8}\cdot\frac{4\omega_S(\Omega_S)^3\omega_D(\Omega)+4\omega_S(\Omega_S)\omega_D(\Omega)^3}{\omega_{\mathrm{rf}}^3}\cdot 2S_XI_Z\right]. \tag{20}$$

As expected, the zeroth-order average Hamiltonian is zero in the $S$-spin operators due to the averaging properties of the rotation by the rf-field. For the case of equal field strength $(a=1)$ the coefficients in front of the odd orders are zero leading to a vanishing contribution from the odd-order average Hamiltonians as expected for a symmetric pulse sequence.[5] However, for $a\neq 1$ all orders contribute to the average Hamiltonian. The second-order dipolar shift is manifest in the first-order average Hamiltonian (which is equivalent to second-order perturbation theory) in form of the $\omega_D(\Omega)^2/(2\omega_{\mathrm{rf}})S_X$ term. The second-order and third-order average Hamiltonians describe higher-order corrections to the Hamiltonian. In the second-order average Hamiltonian the dipolar-coupling term appears as a coupling while the third-order term has again the form of a shift. Depending on the size of the interaction and the rf-field strength it can be necessary to include these higher-order terms to obtain an accurate description of the spin system.

Neglecting the chemical-shielding tensors $(\omega_S(\Omega_S)=0$, $\omega_I(\Omega_I)=0)$ again as in Sec. II A and expanding the powers of the dipolar-coupling tensor $(\omega_D(\Omega)^n)$ in a sum of Legendre polynomials $P_n(\cos\beta)$,[19] we obtain the following expressions for the four orders of average Hamiltonians:

$$\bar{\mathscr{H}}^{(0)} = 0, \tag{21}$$

$$\bar{\mathscr{H}}^{(1)} = -\frac{1-a^2}{a^2+a}\cdot\frac{\delta^2}{2\omega_{\mathrm{rf}}}\cdot S_X\times\left[\frac{1}{20}+\frac{5}{70}P_2(\cos\beta) + \frac{9}{70}P_4(\cos\beta)\right], \tag{22}$$

$$\bar{\mathscr{H}}^{(2)} = \frac{1+a^3}{a^3+a^2}\cdot\frac{\delta^3}{2\omega_{\mathrm{rf}}^2}\cdot 2S_ZI_Z\left[\frac{1}{70}+\frac{3}{28}P_2(\cos\beta) + \frac{27}{385}P_4(\cos\beta)+\frac{9}{154}P_6(\cos\beta)\right], \tag{23}$$

$$\bar{\mathscr{H}}^{(3)}=\frac{1-a^4}{a^4+a^3}\cdot\frac{3\delta^4}{8\omega_{\rm rf}^3}\cdot S_X\Big[\frac{3}{560}+\frac{5}{308}P_2(\cos\beta)+\frac{459}{20020}P_4(\cos\beta)+\frac{9}{770}P_6(\cos\beta)+\frac{9}{1430}P_8(\cos\beta)\Big]. \tag{24}$$

In this representation, the second-order dipolar isotropic shift is clearly manifest in the term $\delta^2/(40\omega_{\rm rf})S_X$. Compared to the basic experiment described in Sec. II A, the shift is scaled by the factor $-(1-a^2)/(a^2+a)$. If the experiment is performed under MAS, the different Legendre polynomials in Eqs. (21)–(24) are scaled by $P_n(\cos\theta)$, where $\theta=54.74°$ is the magic angle at which the sample is spinning.[3] This leads to the scaling factors $P_2(\cos\theta)=0$, $P_4(\cos\theta)=-7/18$, $P_6(\cos\theta)=2/9$, and $P_8(\cos\theta)=11/72$. Under DOR, the different Legendre polynomials in Eqs. (21)–(24) are scaled by $p=P_n(\cos\theta_1)\cdot P_n(\cos\theta_2)$, where $\theta_1=54.74°$ and $\theta_2=30.12°$ are the two angles about which the sample is spinning.[32,33] The numerical scaling factors for these two angles are $p=0$ for $n=2$ and $n=4$, $p\approx-0.086$ for $n=6$, and $p\approx-0.049$ for $n=8$.

Based on the different orders of the average Hamiltonian [Eqs. (21)–(24)] we would expect the second-order average Hamiltonian to become important for the case of equal field strengths for the forward and back rotation ($a=1$) since $\bar{\mathscr{H}}^{(2)}$ is in this case the first nonvanishing term. For a one-bond C–H coupling and a rf-field strength of $\omega_{\rm rf}/(2\pi)=90$ kHz the coupling term is in the order of 50 Hz. However this description is only correct for an isolated two-spin system. If strong homonuclear couplings are present they give rise to the so-called self-decoupling effect[2] and no splitting of the line can be observed.

The pulse sequences in Figs. 3(b) and 3(c) have been analyzed in the same way. The different orders of the average Hamiltonian show the same operator terms as the ones presented in Eqs. (17)–(20), except for an additional $2S_YI_Z$ and $S_Y$ term in $\bar{\mathscr{H}}^{(2)}$. The scaling factors in front of the orders are different and more complicated, but the numerical values for a given effective field strength are very similar.

If we analyze the dipolar isotropic shift for a $CH_2$ three-spin or a $CH_3$ four-spin system, we find that the shift due to the different dipolar couplings is additive. For a $CH_2$ group, we find the following first-order average Hamiltonian:

$$\bar{\mathscr{H}}^{(1)}=-\frac{1-a^2}{a^2+a}\cdot\frac{1}{2\omega_{\rm rf}}\{[\omega_{1D}(\Omega_1)^2+\omega_{2D}(\Omega_2)^2+\omega_S(\Omega_S)^2]\cdot S_X+2\omega_{1D}(\Omega_1)\omega_S(\Omega_S)\cdot 2S_XI_{1Z}+2\omega_{2D}(\Omega_2)\omega_S(\Omega_S)\cdot 2S_XI_{2Z}+2\omega_{1D}(\Omega_1)\omega_{2D}(\Omega_2)\cdot 4S_XI_{1Z}I_{2Z}\}. \tag{25}$$

For a $CH_3$ group, we find that the shift is the sum of the square of all three C–H dipolar couplings scaled by the rf-field strength. The fact that the different carbon atoms show an isotropic shift depending on the number of directly attached protons can be used to separate the different $CH_x$ groups in a 2D spectrum where the $\omega_1$ dimension shows the second-order dipolar shift and the $\omega_2$ dimension displays a normal MAS spectrum. Special consideration must be taken in the case of fast internal motions. These motions can partially average out dipolar couplings as is the case for $CH_3$ groups. If the motion is faster than the cycle time of the pulse sequence, only a scaled dipolar coupling will appear in the dipolar-shift experiment. For $CH_3$ groups, which rotate rapidly about their symmetry axis, the scaling factor is $P_2(\cos 70.5°)\approx 0.33$.

In this context we should analyze other effects which can show up in the same way as the dipolar shift. The most important ones are the isotropic chemical-shift offset ($\Delta\omega_S$) and the anisotropic chemical-shielding tensor ($\omega_S(\Omega_S)$). The chemical-shielding tensor transforms also as a second-rank tensor and therefore gives rise to the same type of effects as the dipolar coupling. The relative size of the effect due to the chemical-shielding tensor can be easily estimated. For an aliphatic carbon atom the anisotropy of the chemical-shielding tensor is usually smaller than 50 ppm leading to a second-order shift which is by a factor of 20 smaller than the shift due to the dipolar coupling at a 100 MHz carbon resonance frequency. The additional shift induced by the isotropic chemical-shift offset can be much larger and cannot always be neglected. However it is very easy to compensate for the offset and correct the obtained second-order shifts by the amount due to the isotropic chemical-shift offset. Based on Eq. (18) we find in first order

$$\bar{\mathscr{H}}^{(1)}=-\frac{1-a^2}{a^2+a}\cdot\frac{\Delta\omega_S^2}{2\omega_{\rm rf}}\cdot S_X. \tag{26}$$

It is important to note that for the pulse sequences of Fig. 3 the rf-field strength is no longer the important factor for the comparison with the mechanical rotation frequency. Here we have to compare the cycle time of the full pulse sequence with the MAS rotation frequency. The above treatment is only valid if the cycle time of the pulse sequence is considerably shorter than the cycle time of the mechanical sample rotation. If the MAS speed approaches the cycle time of the pulse sequence, the consecutive averaging approach breaks down and other theoretical models have to be employed to accurately describe the system. This breakdown has also been observed experimentally (spectra not shown) in the case of the MAS experiment described in the next section. For a rotation frequency of $\omega_r/(2\pi)=10$ kHz the spectra started deviating from the expected form for a cycle time of the pulse sequence of $\tau_c\geqslant 50$ $\mu$s. In addition to the shifted second-order peak, a zero-frequency peak started to appear. This implies that the consecutive averaging approach is in this case only valid for $\omega_r\cdot\tau_c\leqslant\pi$.

It is necessary to discuss the limitations of the average Hamiltonian approach concerning the convergence of the series of Hamiltonians. The condition for convergence is[34,35]

$$\max|\omega_{0i}-\omega_{0j}|\cdot\tau_c\leqslant 2\pi, \tag{27}$$

where $\omega_{0i}$ are the eigenvalues of the Hamiltonian [Eq. (10)]. In our case, assuming that the dipolar coupling tensor is

larger than the chemical-shielding tensor, the maximum transition frequency is $\delta/2=2\pi\cdot 23.3$ kHz for a one-bond C–H coupling. This leads to a maximum cycle time of $\tau_c \leqslant 43$ $\mu$s. For a rf-field strength of $\omega_{\mathrm{rf}}/(2\pi)\geqslant 50$ kHz this condition is usually fulfilled.

The first-order average Hamiltonian of Eq. (18) shows another interesting feature. The cross term between the chemical-shielding tensor and the dipolar-coupling tensor generates a contribution to the first-order average Hamiltonian of the form $\omega_D(\Omega)\omega_S(\Omega_S)/\omega_{\mathrm{rf}}\cdot 2S_X I_Z$. The size of this coupling term depends strongly on the relative orientation of the two tensors and is of importance in the case of continuous-wave decoupling in isolated heteronuclear two-spin systems. A detailed analysis of this effect is in preparation and will be published elsewhere.[36]

## III. EXPERIMENTAL REALIZATION

All experiments were performed on a home-built spectrometer operating at a proton Larmor frequency of 301.2 MHz, using a commercial 4 mm MAS probe assembly from Chemagnetics. As a test sample we used $^{13}$C $\alpha$-labeled alanine which was diluted 1:5 with unlabeled alanine to reduce homonuclear $^{13}$C–$^{13}$C interactions. In all experiments the pulsed version of the nutation sequence [Fig. 3(c)] was used rather than the power-switched version [Fig. 3(a)]. The practical advantages of the pulsed versions are that only one pulse length needs to be calibrated and that the compensation of the basic nutation frequency is superior to that obtained with the power-switched version. The delay $\Delta_1$ was usually set to the minimum possible value of 0.3 $\mu$s and $\Delta_2$ was varied to obtain spectra with different shifts. This version of the pulse sequence ensures that the timing of the forward and backward rotation is the same and experimentally produced a much better compensation of the basic nutation frequency than the sequence shown in Fig. 3(b). For all experiments, cross polarization (CP) (Refs. 2, 3, 37) was used to increase the sensitivity and to shorten the recycle delay. The decoupling field strength on the protons in all experiments was ~75 kHz and the MAS frequency was controlled by a home-built spinning-speed controller.

Figure 4(a) shows the pulse sequence used to record the 2D spectra. Sign discrimination in $\omega_1$ was achieved by the States method.[38] This was implemented by recording two different sets of spectra with and without the first $(\pi/2)_x$-pulse on the $S$-channel. Before running the experiments a tune-up of the phases and amplitudes of the four different quadrature channels of the spectrometer was performed.[2,39] Care was taken to minimize the effects of phase transients.[2] Theoretical calculations show that such phase transients introduce an additional phase modulation in the $t_1$ domain of the 2D experiment leading to an additional splitting of the line, an effect which was also observed experimentally (Fig. 5). The additional phase modulation was used to experimentally minimize the phase transients by matching the impedance of the probe to that of the amplifier.[2,39] After the tune-up no phase modulations could be observed even after 100 iterations of the sequence. Figure 5 shows the projection onto $\omega_1$ for two different spectra recorded under similar conditions without [Fig. 5(a)] and with [Fig. 5(b)] optimization of the impedance matching of the probe to the amplifier. No dipolar shift is expected since $\Delta_1=\Delta_2=0.3$ $\mu$s in both spectra. The spectrum without tuning of the phase transients [Fig. 5(a)] shows a large splitting due to the additional phase modulation in $t_1$. After minimizing the influence of the phase transients, the spectrum [Fig. 5(b)] shows the expected single sharp line at zero frequency with a half-width at half-height of 175 Hz and a Gaussian line shape. Part of this line broadening is due to the apodization of the signal in $t_1$ by a $\cos^2$-window function and the limited

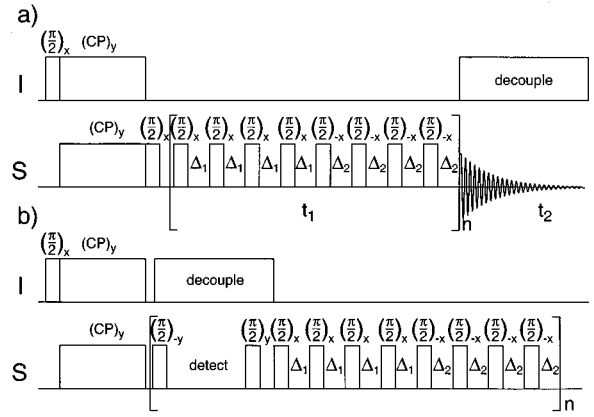


FIG. 4. Two pulse sequences used for measuring the second-order dipolar isotropic shift. Sequence (a) gives a 2D spectrum with a standard 1D MAS spectrum in $\omega_2$ and the nutation spectrum in $\omega_1$. In order to obtain a 1D nutation spectrum, a projection onto $\omega_1$ must be taken. The first $(\pi/2)_x$-pulse is used to generate the second data set for phase-sensitive States processing in $\omega_1$. Sequence (b) is a 1D version with single point acquisition. The $(\pi/2)_y$- and $(\pi/2)_{-y}$-pulses around the detection period are used to flip the $y-z$ plane in which the magnetization is precessing into the $x-y$ plane for detection and back to allow sign discrimination. This sequence requires that the observed line is on-resonance.

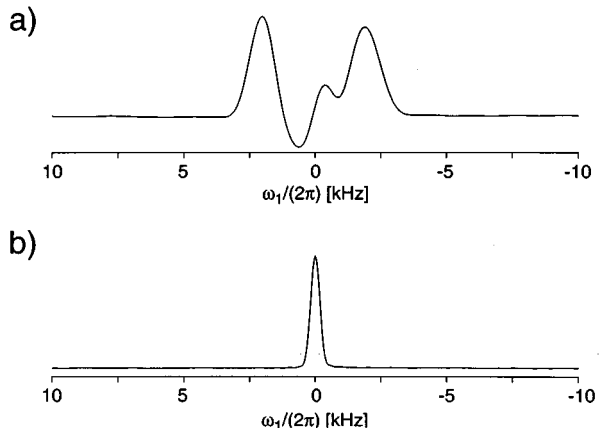


FIG. 5. Influence of phase transients on the $\omega_1$-projection of the 2D dipolar isotropic spectra. (a) is a spectrum recorded without optimizing impedance matching of the probe to the amplifier. The splitting is due to the additional phase modulation induced by the phase transients. (b) shows the spectrum recorded under similar conditions after minimizing the influence of the phase transients. The spectrum shows the expected single sharp line at zero frequency with a half width of the Gaussian line of 175 Hz. Since $\Delta_1=\Delta_2=0.3$ $\mu$s no dipolar isotropic shift is expected.

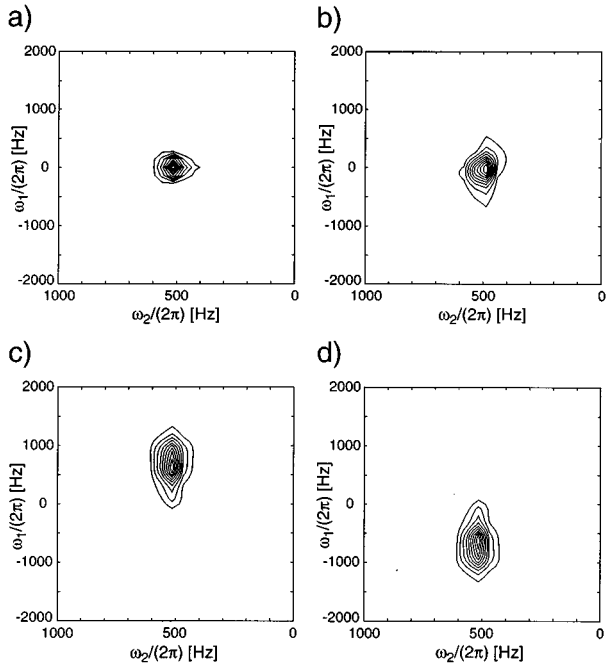


FIG. 6. 2D spectra recorded with the pulse sequence of Fig. 4(a) with a rf-field strength of $\omega_{rf}/(2\pi)\approx 75$ kHz. The CP contact time was 0.5 ms and 128 complex $t_1$ time points with 16 scans each were summed. All spectra show the normal 1D MAS spectrum as the projection onto the $\omega_2$-axis, while the projection onto the $\omega_1$-axis represents the nutation spectrum. (a) was recorded with the delays $\Delta_1$ and $\Delta_2$ set to 0.3 $\mu$s and shows a relatively sharp line at zero frequency in $\omega_1$. In (b) the delays $\Delta_1$ and $\Delta_2$ were set to 4.3 $\mu$s in both the forward and the back rotation pulses. The spectrum shows a slightly broader line due to the lower effective field with the center of gravity still at zero frequency. (c) was recorded with the delay $\Delta_1=0.3$ $\mu$s and $\Delta_2=4.3$ $\mu$s resulting in a positive dipolar shift as well as in a broadening of the line. In (d) the delays $\Delta_1$ and $\Delta_2$ were interchanged, resulting in an inversion of the sign of the shift in $\omega_1$.

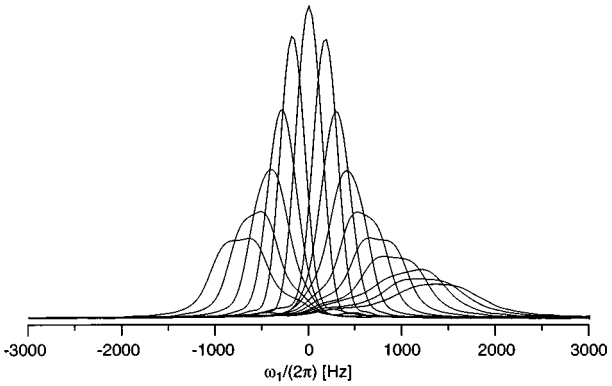


FIG. 7. Series of 1D $\omega_1$-projections demonstrating the dependence of the dipolar isotropic shift on the delays $\Delta_1$ and $\Delta_2$. All spectra were recorded with the pulse sequence of Fig. 4(a). After 2D data processing, a projection onto the $\omega_1$-axis was performed to obtain the 1D spectra. The delay $\Delta_2$ was varied from 0.3 $\mu$s in 0.8 $\mu$s increments to a maximum value of 7.5 $\mu$s resulting in a positive dipolar shift, while $\Delta_1$ was kept constant at 0.3 $\mu$s. In a second set of experiments, the delay $\Delta_1$ was varied from 0.3 $\mu$s in 0.8 $\mu$s increments to a maximum value of 4.3 $\mu$s, leading to a negative dipolar shift, while the delay $\Delta_2$ was kept constant at 0.3 $\mu$s in this series. The two sets of spectra with positive and negative shifts are mirror images as expected.

number of measured $t_1$ points (64 complex). Another spectrum recorded under similar conditions but with 256 complex $t_1$ points exhibited a linewidth of only 90 Hz.

Figure 6 shows 2D spectra demonstrating the dipolar isotropic shift. All spectra were recorded with a rf-field strength of $\omega_{rf}/(2\pi)\approx 75$ kHz, a CP contact time of 0.5 ms, and a spinning speed of 5 kHz. One hundred and twenty-eight complex $t_1$ time points with 16 scans each were added up with a recycle delay of 1 s. After a hypercomplex Fourier transformation the resulting spectra show the expected features (Fig. 6). The projection onto $\omega_2$ shows the standard MAS spectrum in all cases while the projection onto $\omega_1$ represents the dipolar-shift or nutation spectrum. For the spectrum shown in Fig. 6(a), the delay $\Delta_1=\Delta_2=0.3$ $\mu$s resulted in no dipolar shift and a relatively sharp line at zero frequency in $\omega_1$. The spectrum in Fig. 6(b) was recorded with delays $\Delta_1=\Delta_2=4.3$ $\mu$s inserted into the forward and the back rotation of the sequence shown in Fig. 4(a) leading to a reduced effective field strength but to no dipolar isotropic shift since the effective field for both rotations is the same. The resonance line is slightly broader in the $\omega_1$ dimension due to the lower average field strength but is still at zero frequency. For the spectrum shown in Fig. 6(c) the delays were set to $\Delta_1=0.3$ $\mu$s and $\Delta_2=4.3$ $\mu$s leading to a positive dipolar shift and a broadening of the spectrum due to the $P_4(\cos\beta)$ term which is not averaged out by the magic-angle sample spinning. For the spectrum in Fig. 6(d), the delays $\Delta_1$ and $\Delta_2$ were interchanged ($\Delta_1=4.3$ $\mu$s, $\Delta_2=0.3$ $\mu$s) resulting in an inversion of the sign of the dipolar shift. The same inversion of the sign can be achieved by shifting all the phases of the nutation sequence by 180°.

Figure 7 shows a set of 1D $\omega_1$ projections in order to demonstrate the dependence of the dipolar shift on the delays $\Delta_1$ and $\Delta_2$. All 2D spectra were recorded with the same parameters as the 2D spectra shown in Fig. 6 ($\omega_{rf}/(2\pi)=75$ kHz, $\omega_r/(2\pi)=5$ kHz, $\tau_{CP}=0.5$ ms, 128 complex $t_1$ points with 16 scans each), using the pulse sequence of Fig. 4(a). After 2D processing, a sum-projection along $\omega_1$ was calculated over the width of the peak. This resulted in the 1D spectra shown in Fig. 7. The delay $\Delta_2$ was varied from 0.3 $\mu$s in steps of 0.8 $\mu$s to a maximum value of 7.5 $\mu$s while the delay $\Delta_1$ was kept constant at 0.3 $\mu$s, leading to a positive dipolar shift. At the same time, the broadening of the line also increases with increasing shift as expected due to the $P_4(\cos\beta)$-term which is not averaged out by MAS. In a second set of experiments, the delay $\Delta_1$ was varied from 0.3 $\mu$s in increments of 0.8 $\mu$s to a maximum value of 4.3 $\mu$s while the delay $\Delta_2$ was kept constant at 0.3 $\mu$s resulting in a negative dipolar shift. The two sets of spectra with positive and negative shifts are mirror images, as expected.

The experiment can be implemented not only in the 2D fashion discussed so far [Fig. 4(a)], but also as a 1D experiment with single-point detection.[40] The sequence used to implement the 1D version of the experiment is shown in Fig. 4(b). During the detection period the magnetization which precesses in the $y-z$-plane during the nutation sequence is flipped into the $x-y$-plane by the first $(\pi/2)_{-y}$-pulse and after the detection rotated back into the $y-z$-plane by a

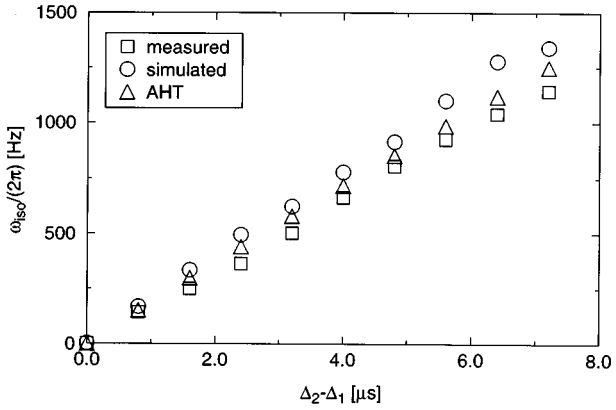


FIG. 8. Isotropic shifts for the spectra shown in Fig. 7 as a function of the difference of the delays $\Delta_2$ and $\Delta_1$. The isotropic shifts were calculated for the experimental spectra (□) by calculating the center of gravity for the 1D spectra. The numerical simulations (○) were performed using small step integration of the equation of motion to describe the time dependence of the Hamiltonian due to the MAS sample rotation under the pulse sequence of Fig. 3(c). The average Hamiltonian calculations (△) include only the first-order average Hamiltonian for the sequence shown in Fig. 3(c).

$(\pi/2)_y$-pulse. The sequence requires that the line in question is on-resonance because of the chemical shift evolution during the detection time. The sequence can be modified by inserting an additional $\pi$-pulse in the middle of the detection period to refocus the chemical shift. The 1D sequence did not work as well experimentally as the 2D sequence of Fig. 4(a). The signal to noise ratio of the spectra was considerably lower than that for the 1D $\omega_1$ projections recorded in the same amount of time.

Figure 8 shows a comparison of the isotropic dipolar shift as a function of the difference of the two delays $\Delta_2-\Delta_1$ for the measurements, numerical simulations and first-order average Hamiltonian theory. The measured values were obtained by calculating the center of gravity of the spectra shown in Fig. 7. As expected, the isotropic shift increases with increasing values of $\Delta_2-\Delta_1$. The numerical simulations were performed using small-step integration of the Liouville-von-Neumann equation because of the time-dependence of the Hamiltonian due to the MAS sample rotation. Five thousand time steps were calculated for a full rotor cycle leading to a time resolution of 40 ns. The experimental pulse sequence of Fig. 3(c) was used for the simulations and 538 different powder orientations were calculated. The C–H distance was taken from a neutron diffraction measurement of alanine.[41] This value was corrected for the different vibrational averaging of neutron diffraction and NMR (Ref. 42) resulting in $r_{CH}=1.104$ Å. The isotropic dipolar shifts of the simulated spectra were calculated in the same way as for the experimental data. The shifts from the numerical simulations are consistently too high. There are two uncertain parameters in the simulation, the C–H distance and the rf-field strength. One possible reason for this systematic error could be the numerical value for the C–H distance which was used in the simulations. However, an increase of 3% in the bond length is necessary to account for the difference between the simulated and measured shifts. In the numerical simulations the pulse sequence was implemented by ideal square-wave pulses with a finite length. In the experiment, however, all pulses have a finite rise and decay time leading to a higher peak rf-field strength in the experiment than it is calculated from the $\pi/2$-pulse length. The rise and decay times can explain the discrepancies between experiment and simulation because the second-order shift depends on the inverse of the field strength. The higher peak rf-field strength in the experiment will lead to a smaller isotropic shift compared to the simulations. The points shown for the average Hamiltonian theory include only the first-order term. They were also calculated for the experimental pulse sequence of Fig. 3(c) and here the isotropic shift can be obtained analytically. For the dipolar coupling constant the same value $(\delta/(2\pi)=44.4$ kHz) as in the numerical simulations was used.

To show the potential of this new method as a tool to separate CH, $CH_2$, and $CH_3$ groups, spectra of two different samples under identical conditions were recorded. The first sample is a 14 amino acid peptide from the Prion protein (PrP) corresponding to residues 109 to 122 of Syrian Hamster PrP with the sequence MKHMAGAAAAGAVV.[43,44] A mixture of two different $^{13}C$ labels on the methyl and alpha carbon of alanine-115 was used. The second sample was a Gly–Gly dipeptide with a $^{13}C$ label at glycine-2 $^{13}C_\alpha$. The spinning speed was set to $\omega_r/(2\pi)=6080$ Hz, the field strength was $\omega_{rf}/(2\pi)=75.6$ kHz, and the CP contact time was set to 2.5 ms. Two hundred and fifty-six (14 residue peptide) or 64 (Gly–Gly) scans were added up for each of the 64 complex $t_1$ times using the pulse sequence of Fig. 4(a). Figure 9(a) shows the resulting spectra for $\Delta_1=\Delta_2=0.3$ $\mu$s showing, as expected, no dipolar shift for all peaks. The spectra in Fig. 9(b) were recorded with $\Delta_1=0.3$ $\mu$s and $\Delta_2=2.7$ $\mu$s and show the expected shifts. The peak of the $CH_2$ group has the largest shift and its resonance is considerably broader than the line of the CH group. The $CH_3$ group shows the smallest shift as a result of the partial averaging of the dipolar coupling due to the fast rotation of the $CH_3$ group about its symmetry axis. The motion leads to a scaling of the dipolar coupling by $P_2(\cos 70.5°)\approx 0.33$ and therefore to a reduction of the shift due to a single proton to roughly 1/9 compared to the shift of a rigid CH group. Because there are three equivalent protons, the total shift for a $CH_3$ group is roughly 1/3 of the shift of a rigid CH group. The influence of the chemical-shift offset over the observed range is very small. Based on the first-order average Hamiltonian [Eq. (26)] the second-order shift induced by an isotropic chemical-shift offset of 2000 Hz is less than 20 Hz and can therefore be neglected. The characteristic shifts of the different groups in $\omega_1$ together with the high resolution in $\omega_2$ allow the separation of the CH, $CH_2$, and $CH_3$ groups in a 2D spectrum.

## IV. CONCLUSIONS

We have shown that second-order dipolar shifts in the rotating frame can be substantially larger than the second-order effects due to truncation of the dipolar coupling by the Zeeman field. The shifts can be on the order of 1000 Hz, compared to a shift of several Hertz in the case of the

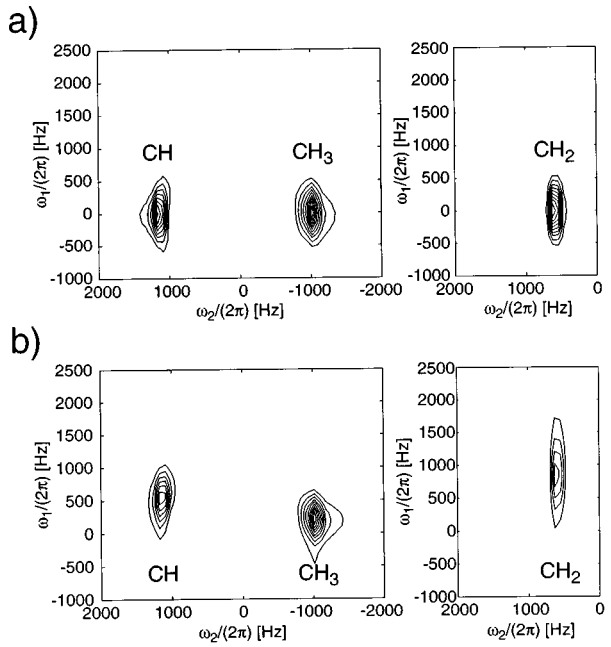


FIG. 9. Comparison of the second-order dipolar isotropic shift in the rotating frame for a CH, a $CH_2$ and a $CH_3$ group. The spectra in (a) were measured under MAS conditions ($\omega_r/(2\pi)=6070$ Hz) with the pulse sequence of Fig. 4(a) with both delays set to $\Delta_1=\Delta_2=0.3$ $\mu$s and a field strength of $\omega_{rf}/(2\pi)=75$ kHz. For the spectra in (b) the delays were set to $\Delta_1=0.3$ $\mu$s and $\Delta_2=2.7$ $\mu$s. As expected there is no dipolar shift for all three lines in (a). In (b), however, the $CH_2$ group shows the largest shift, roughly twice the size of the shift arising from the CH group. The $CH_3$ group shows the smallest shift due to the partial averaging of the dipolar couplings from the fast rotation of the $CH_3$ group about the symmetry axis.

laboratory-frame experiment. The second-order effect shows up as a combination of an isotropic shift, a second-rank tensor, and a fourth-rank tensor powder pattern. By using a modified pulse sequence, the effects of rf-field inhomogeneity can be reduced considerably. The simulated and experimental spectra show the expected isotropic shift, a second-rank tensor component, and a fourth-rank tensor component leading to inhomogeneously broadened spectra. The powder broadenings can be averaged out by using MAS or DOR techniques.

We have demonstrated one possible application of this new technique, namely the separation of CH, $CH_2$, and $CH_3$ groups in a 2D MAS spectrum due to their different second-order dipolar shifts in the $\omega_1$ domain of a 2D spectrum. Combined with the high resolution of a MAS spectrum in the $\omega_2$ domain, such a spectrum can provide information for the assignment of $^{13}C$ resonances in larger molecules. However, care has to be taken to compensate for isotropic chemical-shift offsets or second-order shifts due to the chemical-shielding tensor. For aliphatic carbon atoms the chemical-shielding tensor is usually small enough that it can be neglected, and the compensation for the chemical shift offset can be calculated analytically in a straightforward manner. Implemented under DOR, the new technique could be used to filter the carbon atoms according to the number of directly-attached protons using the isotropic part of the shift. Future work to explore the implementation of this experiment under DOR is under way in our laboratory.

## ACKNOWLEDGMENTS

This work was supported by the Director, Office of Energy Research, Office of Basic Energy Sciences, Materials Sciences Division, U.S. Department of Energy, under Contract No. DE-AC03-76SF00098. We would like to thank Dr. Scott Smith for his help with the simulation package GAMMA. Tilo Levante, Marc Baldus, Professor Dr. Beat Meier, and Professor Dr. Richard Ernst provided the code for the Floquet simulations within the GAMMA simulation package. Many stimulating and helpful discussions with Dr. Jonathan Jones and experimental support by Jonathan Heller are gratefully acknowledged. We would also like to thank Susan De Paul for carefully reading and correcting the manuscript. M.E. thanks the Deutsche Forschungsgemeinschaft for a postdoctoral fellowship (Grant Er 214/1-1).

[1] A. Abragam, *Principles of Nuclear Magnetism* (Clarendon, Oxford, 1961).
[2] U. Haeberlen, *High Resolution NMR in Solids-Selective Averaging* (Academic, New York, 1976).
[3] M. Mehring, *Principles of High Resolution NMR in Solids* (Springer, Berlin, 1983).
[4] U. Haeberlen and J. S. Waugh, Phys. Rev. **175**, 453 (1968).
[5] R. R. Ernst, G. Bodenhausen, and A. Wokaun, *Principles of Nuclear Magnetic Resonance in One and Two Dimensions* (Clarendon, Oxford, 1987).
[6] D. Freude and J. Haase, NMR Basic Principles and Progress **29**, 1 (1993).
[7] K. T. Mueller, B. Q. Sun, G. C. Chingas, J. W. Zwanziger, T. Terao, and A. Pines, J. Magn. Reson. **86**, 470 (1990).
[8] A. Llor and J. Virlet, Chem. Phys. Lett. **152**, 248 (1988).
[9] A. Samoson, E. Lippmaa, and A. Pines, Mol. Phys. **65**, 1013 (1988).
[10] L. Frydman and J. S. Harwood, J. Am. Chem. Soc. **117**, 5367 (1995).
[11] F. Bloch and A. Siegert, Phys. Rev. **57**, 522 (1940).
[12] A. Lösche, Ann. Phys. (Leipzig) **20**, 178 (1957).
[13] S. A. Vierkötter, J. Magn. Reson. A **118**, 84 (1996).
[14] D. L. VanderHart, J. Chem. Phys. **84**, 1196 (1986).
[15] M. P. Augustine, K. W. Zilm, and D. B. Zax, J. Chem. Phys. **98**, 9432 (1993).
[16] F. A. L. Anet and D. J. O'Leary, Concepts in Magn. Reson. **3**, 193 (1991).
[17] J. B. Robert and L. Wiesenfeld, Phys. Rep. **86**, 363 (1982).
[18] R. Tycko, J. Chem. Phys. **92**, 5776 (1990).
[19] D. M. Brink and G. R. Satchler, *Angular Momentum* (Clarendon, Oxford, 1993).
[20] E. R. Andrew, A. Bradbury, and R. G. Eades, Nature **182**, 1659 (1958).
[21] E. R. Andrew, A. Bradbury, and R. G. Eades, Nature **183**, 1802 (1959).
[22] I. J. Lowe, Phys. Rev. Lett. **2**, 285 (1959).
[23] J. H. Shirley, Phys. Rev. B **138**, 979 (1965).
[24] S. A. Smith, T. O. Levante, B. H. Meier, and R. R. Ernst, J. Magn. Reson. A **106**, 75 (1994).
[25] M. Baldus, T. O. Levante, and B. H. Meier, Z. Naturforsch. **49a**, 80 (1994).
[26] V. B. Cheng, H. H. Suzukawa, and M. Wolfsberg, J. Chem. Phys. **59**, 3992 (1973).
[27] A. Schmidt and S. Vega, J. Chem. Phys. **96**, 2655 (1992).
[28] T. O. Levante, M. Baldus, B. H. Meier, and R. R. Ernst, Mol. Phys. **86**, 1195 (1995).
[29] A. C. Kolbert and S. L. Gann, Chem. Phys. Lett. **224**, 86 (1994).
[30] S. Wolfram, *Mathematica-A System for Doing Mathematics by Computer* (Addison–Wesley, Reading, 1991).
[31] S. Boentges (private communication).
[32] B. Q. Sun, J. H. Baltisberger, Y. Wu, A. Samoson, and A. Pines, Solid State NMR **1**, 267 (1992).

[33] B. F. Chmelka and J. W. Zwanziger, NMR Basic Principles and Progress **33**, 79 (1994).
[34] M. M. Maricq, J. Chem. Phys. **86**, 5647 (1987).
[35] M. M. Maricq, Adv. Magn. Reson. **14**, 151 (1990).
[36] M. Ernst, S. Bush, A. C. Kolbert, and A. Pines (unpublished).
[37] A. Pines, M. G. Gibby, and J. S. Waugh, J. Chem. Phys. **56**, 1776 (1972).
[38] D. J. States, R. A. Haberkorn, and D. J. Ruben, J. Magn. Reson. **48**, 286 (1982).
[39] B. C. Gerstein, Philos. Trans. R. Soc. London, Ser. A **299**, 521 (1981).
[40] J. S. Waugh, L. M. Huber, and U. Haeberlen, Phys. Rev. Lett. **20**, 180 (1968).
[41] M. S. Lehmann, T. F. Koetzle, and W. C. Hamilton, J. Am. Chem. Soc. **94**, 2657 (1972).
[42] E. R. Henry and A. Szabo, J. Chem. Phys. **82**, 4753 (1985).
[43] S. B. Prusiner, Science **252**, 1515 (1991).
[44] S. B. Prusiner, Biochem. **31**, 12277 (1992).